1606 Vol. 43, No. 7 / 1 April 2018 / Optics Letters Letter

Optics Letters

Line-scan spectrum-encoded imaging by dual-comb interferometry

Chao Wang,[1] Zejiang Deng,[1] Chenglin Gu,[1] Yang Liu,[1] Daping Luo,[1] Zhiwei Zhu,[1] Wenxue Li,[1,*] and Heping Zeng[1,2]

[1]State Key Laboratory of Precision Spectroscopy, East China Normal University, Shanghai 200062, China
[2]e-mail: hpzeng@phy.ecnu.edu.cn
*Corresponding author: wxli@phy.ecnu.edu.cn

Received 22 January 2018; accepted 18 February 2018; posted 26 February 2018 (Doc. ID 320189); published 29 March 2018

Herein, the method of spectrum-encoded dual-comb interferometry is introduced to measure a three-dimensional (3-D) profile with absolute distance information. By combining spectral encoding for wavelength-to-space mapping, dual-comb interferometry for decoding and optical reference for calibration, this system can obtain a 3-D profile of an object at a stand-off distance of 114 mm with a depth precision of 12 μm. With the help of the reference arm, the absolute distance, reflectivity distribution, and depth information are simultaneously measured at a 5 kHz line-scan rate with free-running carrier-envelope offset frequencies. To verify the concept, experiments are conducted with multiple objects, including a resolution test chart, a three-stair structure, and a designed "ECNU" letter chain. The results show a horizontal resolution of ∼22 μm and a measurement range of 1.93 mm. © 2018 Optical Society of America

OCIS codes: (050.1950) Diffraction gratings; (110.6880) Three-dimensional image acquisition; (330.6130) Spatial resolution.

https://doi.org/10.1364/OL.43.001606

Non-contact surface mapping with depth information at a distance is interesting in diverse applications, including biomedical imaging, industrial metrology, manufacturing, artifact documentation, and preservation [1]. Combining single-spot absolute distance measurements with mechanical scanning is the direct and most common method for providing accurate surface profiling and mapping [2–6]. During the past decade, the optical frequency comb has proven to be very powerful in the field of distance metrology [7]. It has been developed as an ideal light source or frequency calibration in various absolute distance measurement methods, such as multiple-wavelength interferometry [8], time-of-flight measurements [9], dispersive interferometry [10], and dual-comb interferometry [11]. Meanwhile, no-scanning 3-D distance measurements have also been demonstrated with one chirped optical frequency comb [12,13]. These methods have distinct merits and drawbacks and find their own unique applications. Dual-comb interferometry, also known as multi-heterodyne interferometry in the field of precision spectroscopy [14], has attracted greater attention than other methods because of its down-sampling conversion, measurement at continuous distance, and further extendible non-ambiguous range. It permits the measurement of the amplitude and phase distribution of individual comb modes in the radio frequency (RF) region where slow detectors and electronics can be used for fast Fourier transform analysis. Much work that focuses on single-spot distance measurement with better ranging resolution, high update rate, high signal-to-noise ratio, and extended non-ambiguity range has recently been reported [15,16].

Spectral encoding is a promising technique for scan-less imaging with high frame rates. Since its inception, this technique has achieved widespread application in endoscopy [17] and time-stretch imaging [18]. By using a spatial disperser with wavelength-to-space mapping, the spatial information of an object can be encoded onto the broadband spectrum of an ultrafast pulse laser, enabling rapid image acquisition without mechanical scanning devices which limit the scan rate, precision, and utility. Running in one-dimensional (1-D) spectral-encoding mode, spectrally encoded endoscopy enables miniature, small-diameter endoscopic probes for minimally invasive imaging [19]. Combining spectral encoding with the time-stretch technique and single-pixel high-speed photodetector, serial time-encoded amplified microscopy has achieved ultrafast imaging frame rates beyond 1 MHz [20]. With additional interferometric techniques, time-stretch quantitative phase imaging is demonstrated to retrieve depth information or index difference with nanometer resolution and high frame rates [21,22]. Since dual-comb interferometry is a superior technique for phase measurement, it is a novel method to combine dual-comb interferometry with spectral encoding. Recently, Hase *et al.* demonstrated proof-of-principle experiments with tightly locked dual combs, showing potential applications in precision measurements [23,24]. Taking the advantages of both techniques enables the system to capture 3-D images with high-ranging resolution, high update rate and lower scanning dimension.

In this Letter, we study, to the best of our knowledge, a novel design of a line-scan 3-D imaging system by combining dual-comb interferometry, spectral encoding, and the optical reference technique. Three parameters, including the 1-D reflectivity distribution, the relative depth information, and absolute distance, can be obtained at the same time using just two oscillators with free-running CEOs.

A schematic of the system is depicted in Fig. 1(a). In temporal optical scanning, we employ a pair of stabilized femtosecond laser combs with pulse trains of slightly different repetition rates (f_r and $f_r + \Delta f_r$). The pulses from the signal light (SL) are split into the reference arm and measurement arm, which contains a user-defined beam expander. The key feature of this method is mapping the object's X-axis reflectivity distribution and Z-axis depth information onto the signal pulse's spectral magnitude and phase, respectively. This is achieved by mapping the spectrum into a 1-D space using a spatial disperser. (Details are shown in Fig. 2.) The encoding occurs when the spatially dispersed pulses reflect off the object. After converting the image-encoded spectrum into the RF region using the dual-comb interferometry method, the decoding and calculation are accomplished using the time interval of the interferograms, the spectral magnitude difference, and the phase difference.

The time-domain picture captured by the detectors is shown in Fig. 1(b). An entire "scan" of the local oscillator (LO) reference pulse across the signal pulse is accomplished every 200 μs in real time and every ~2 ns in effective time. An orthogonal polarization method is designed to separate the measurement and reference interferograms, showing no dead zones in the measurement range. By using the time-of-flight method, and judging the time delay between adjacent interferogram pulses, the absolute distance can be obtained.

Furthermore, by Fourier transforming the digitized pulses with the same time window near the peak position [green box in Fig. 1(b)], the RF spectra of both interferograms can be obtained, as shown in Fig. 1(d). Given the RF spectrum data sets with magnitudes and phases, the 1-D reflectivity distribution of the object is defined by the spectral magnitude ratio between the measurement and reference, as shown in Fig. 1(d). In addition, the relative depth distribution L along the X-axis is related to the phase slope $d\varphi(\nu)/d\nu$ by [15]

$$L = \left(\frac{c}{4\pi}\right)[d\varphi(\nu)/d\nu], \tag{1}$$

where c is the speed of light, and ν is the optical frequency. Therefore, both the 1-D reflectivity distribution and Z-axis depth information are obtained in the updated time of 200 μs. By scanning the target along the Y-axis, 3-D imaging with absolute distance can then be realized. A proof-of-principle experiment is demonstrated by scanning the object to the place where there is a stair-step structure, and calculating the depth information (0.8 mm). The stair-step structure with two surfaces is successfully retrieved, as shown in Fig. 1(f).

Next, we demonstrate the detailed operation and discuss key performance factors of the imaging system with the experimental setup shown in Fig. 2. The light sources for the SL and LO are two homemade Yb-doped fiber lasers [25]. The repetition rates of both sources can change in the range of 480 ± 20 MHz using a piezoelectric transducer (PZT) actuator coupled to a motorized stage inserted within the cavities. The two lasers share similar

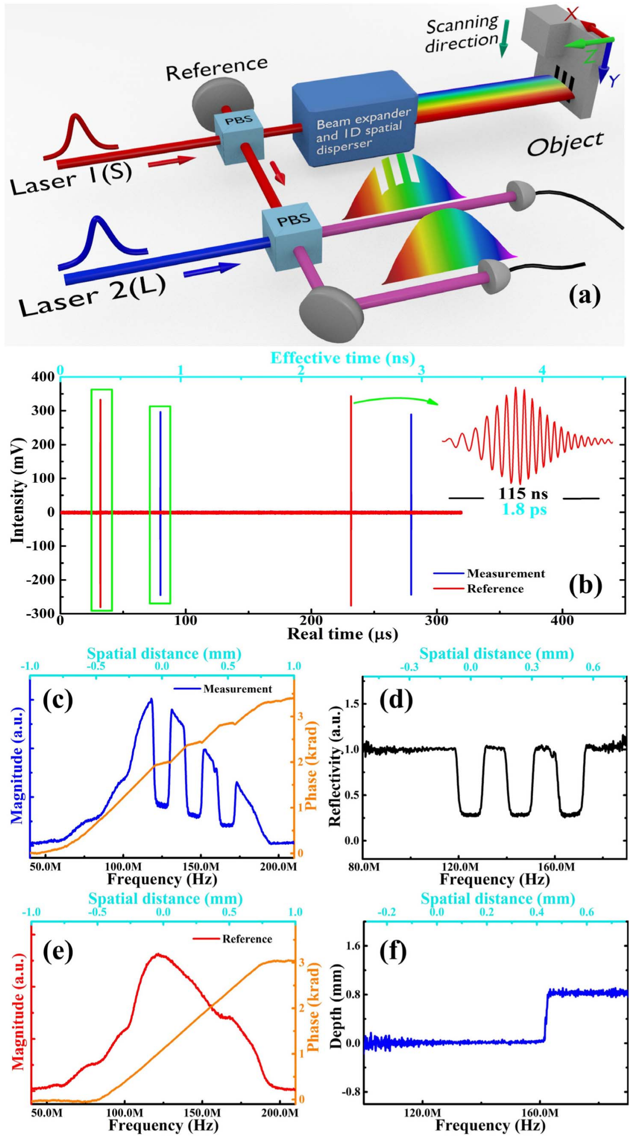

Fig. 1. Imaging method. (a) Schematic of line-scan 3-D imaging system. (b) Captured reference interferogram (red) and measurement interferogram (blue). The inset shows the zoomed-in view of the interferogram. Spectral magnitude and unwrapped phase of (c) the measurement interferogram and (e) the reference interferogram. (d) Calculated reflectivity image. (f) Obtained depth curve of the "stair-step" structure.

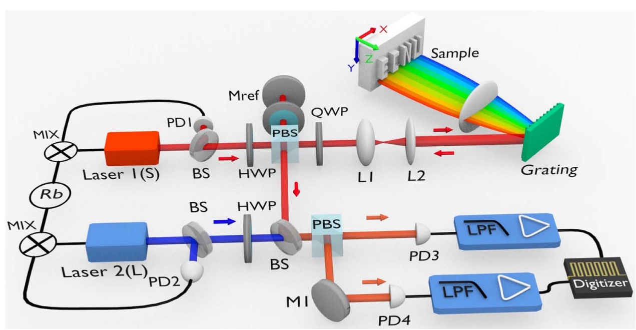

Fig. 2. Schematic of the experimental setup. Rb, rubidium clock; PD, photodetector; BS, beam splitter; HWP, half-wave plate; QWP, quarter-wave plate; PBS, polarization beam splitter; L, lens; M, mirror; LPF, low-pass filter; MIX, mixer.

characteristics such as average output power of ~400 mW, pulse duration of ~340 fs, and spectral bandwidth of ~25 nm. The repetition rates of the two lasers ($f_{\mathrm{rep1}} = 480$ MHz + 5 kHz for SL and $f_{\mathrm{rep2}} = 480$ MHz for the LO) are locked to a rubidium (Rb) atomic clock using two feedback loops.

The pulses from the SL are split into the reference and measurement arms using a half-wave plate (HWP) and a polarizing beam splitter (PBS). In the measurement arm, a pair of achromatic lenses with different focal lengths ($f_1 = 19$ mm and $f_2 = 50$ mm) are used to expand the beam diameter to form a probe beam. This expanded beam is spatially dispersed by a diffraction grating (groove density of 1000 lines/mm) and then collimated by an achromatic lens (focal length of 30 mm), generating a 1-D spectral shower on the sample. This spectral shower has a length of ~1.5 mm along the X-axis. After spectral encoding with the sample profile and depth information, the pulses propagate back through the same optics and are combined with orthogonally polarized pulses from the reference arm at the PBS using two quarter-wave plates (QWPs). Meanwhile, using an HWP, a beam splitter (BS) and a PBS, the pulses from the LO are split into two parts and interfere with the reference and measurement pulses, respectively, generating orthogonally polarized interferograms that are detected without overlapping by two photodetectors (PD3 and PD4). After passing through a low-pass filter and electric amplifier, the output signals from the two PDs are individually digitized using a 12 bit data acquisition card (ATS9360, Alazartech) synchronized to the Rb clock. The interferograms from two channels are recorded with 800 MHz bandwidth and 1.8 GHz sampling rate. About 2 mW pulses in each channel are coupled into fiber-pigtailed PDs which have 1.5 m fiber pigtail and work in the linear detection region.

The performance of the absolute distance measurement is first tested while the sample is fixed at ~114 mm away. In the short-distance measurement, the uncertainty is mainly attributable to the uncertainty of the repetition rate. Figure 3(a) shows the phase noise of f_r in both the free-running and phase-locked states using a signal source analyzer (R&S FSWP). The inset shows the integrated phrase noise (IPN) for two states. The calculated values from 1 Hz to 10 MHz are 62.4 and 1.22 mrad, respectively. However, the low-frequency part is limited by the phase noise of the RF signal generator (SMB100A, R&S). Since the control bandwidth of the PZT is limited at ~500 Hz, some unwanted phase noise induced by the feedback loop adds into the cavity from 500 Hz to ~7 kHz. To avoid the influence of added phase noise, under the premise of no aliasing in the RF spectrum, we increased the frequency difference to 5 kHz.

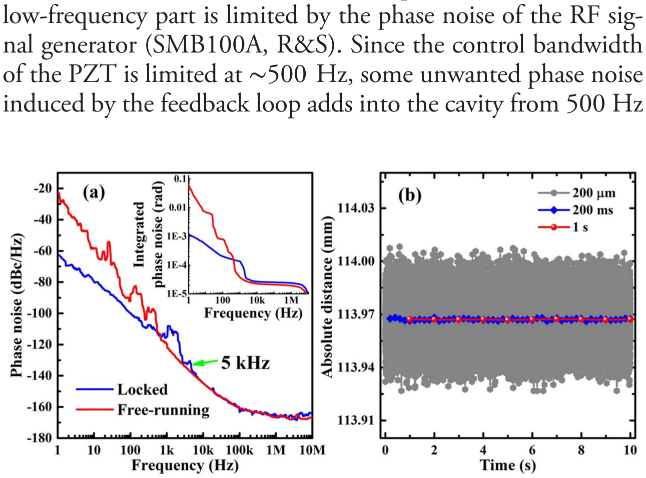

Fig. 3. (a) Phase noise of the repetition rate f_r in a free-running mode (red curve) and 2-th harmonic phase-locked state (blue curve). The inset shows the responding IPN. (b) Stability variation with different averaging times.

As shown in Fig. 3(b), the stability of the signal (standard deviation) varies with averaging time: 11.7 μm for 200 μs, 490 nm for 200 ms, and 159 nm for 1 s with the corresponding mean distance of 113.97 mm. Better performance can be realized using PZTs with broader bandwidths and a signal generator with lower phase noise in the low-frequency region.

To experimentally verify the wavelength-to-space mapping and investigate the spatial resolution, a resolution test chart (1951 USAF) is placed at the focal position to act as the sample. By scanning the sample along the Y direction with a step size of 5 μm, the two-dimensional (2-D) distribution of reflectivity is mapped, as shown in Fig. 4. The field of view is as large as ~1.06 mm × 1.25 mm with a pixel size of 1000 × 250. Since the CEOs are not actively controlled, the central positions of the magnitude curves in both Figs. 1(c) and 1(d) have fluctuation when scanning the sample. If only using the measurement data set to reconstruct the reflectivity image, there's inevitable distortion on the profile as shown in Fig. 4(a). Using the reference arm can effectively align the positions because the fluctuations of both arms are mostly the same and can be cancelled, as shown in Fig. 4(b). The fluctuation (from both f_r and f_{CEO}) with a rate lower than 5 kHz can be removed by actively aligning with the optical reference method. The main limiting factor for the resolution in our imaging system is the beam diameter of the individual mode on the sample [26]. The spatial resolution can be evaluated by

$$\delta x = \frac{4 f \lambda_0}{\pi D}, \tag{2}$$

where f is the focal length of the objective lens, D represents the input beam diameter, and λ_0 is the center wavelength (1040 nm). In our case, after the beam expander, the beam diameter is ~2 mm. Thus, the estimated spatial resolution δx is ~19.8 μm. In practice, Element 4 of Group 5 on the resolution test chart is resolved, indicating a spatial resolution of ~22 μm that is reasonably close to the calculated value. We use seven groups of data sets to average and smooth the reflectivity curve in each row. The zoomed-in view of the smallest element is displayed in the lower inset.

To further verify the calculation of depth information, a homemade three-stair structure and a designed "ECNU" letter chain are utilized as the sample. We increase the focal length of the lens before the sample to 50 mm to sufficiently image the sample with a larger horizontal range of 2.28 mm. The three-stair sample is made by stacking two glass blocks

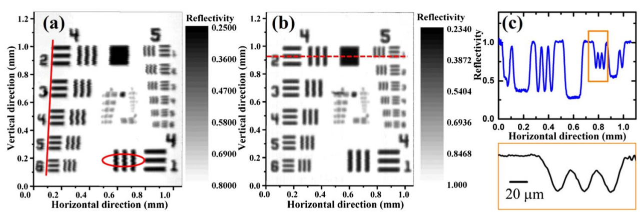

Fig. 4. 2-D reflectivity images of a resolution test chart (a) without and (b) with optical reference. (c) Single scan of the red dashed line as indicated in (b). Inset shows the zoomed-in view of the smallest element.

(1.5 mm × 2.5 mm) with different thicknesses on a plate mirror, forming three surfaces with different step heights, as shown in the inset of Fig. 5(b). Figure 5(a) shows the 3-D image reconstructed by decoding the depth information using Eq. (1). A cross-section extracted from the 3-D image (white dashed line) is plotted in Fig. 5(b), showing three clear stair steps with different heights (0, 600, and 800 μm). The corresponding standard deviation of the middle step is 12 μm. The uncertainty increases a little to 18.7 μm in the other two steps, mainly due to lower signal to noise ratios in the RF spectrum. The overall shape or sink along the boundaries can be removed as no truth data are available.

Finally, a silicon step block with the ECNU logo is used to test the performance of this system in a non-ideal situation where some parts of the sample have low reflectivity. The sample is fabricated on a polished silicon substrate using a deep etching process, forming a two-step structure with the ECNU logo raised. Using the decoding method mentioned above, the 2-D reflectivity distribution and 3-D surface profile are obtained at the same time, as shown in Figs. 5(c) and 5(d). Note that there is a large area around the logo that has a reflectivity of less than 20%, which is mainly caused by the poor flatness in the imperfect etching in Fig. 5(d), we artificially remove the random noise spikes in the low-reflectivity region (lower than 50%) and uniformly set the depth as 100 μm for a clear contrast between the logo surface (red) and bottom surface (green). The height difference of 220 μm is clearly demonstrated with a standard deviation of 12 μm. The acquisition time of this picture is only 252 ms. It is interesting to find that a small and insular area with good flatness inside the letter C is recognized, indicating that this method is useful for measuring discrete surfaces with different depth.

In conclusion, we have proposed and experimentally demonstrated line-scan spectrum-encoded 3-D imaging based on dual-comb interferometry. 3-D surface profiles with absolute distance measurements are achieved in a single measurement. The stability of the system in the Z-axis is demonstrated with an uncertainty of 12 μm that can be reduced to 159 nm for 1 s averaging time. Clear 3-D structure profiles are also obtained with a horizontal resolution of ~22 μm and an imaging range of 1.93 mm. Better spatial resolution, even mode-resolved microscopy, is possible by using a microscope objective and completely locked dual-comb lasers. In addition, the present imaging technique can be further extended to scan-less 3-D imaging by employing a 2-D spatial disperser based on a virtually imaged phased array.

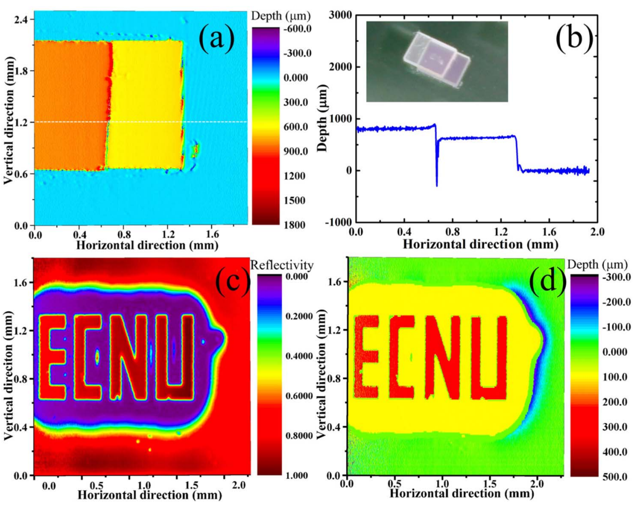

Fig. 5. (a) 3-D surface profile with depth structure of a stair-step sample. (b) Single scan of the white dashed line as indicated in (a). The inset shows the picture captured with a camera. (c) 2-D reflectivity image of the "ECNU" letter chain. (d) 3-D surface profile with depth information.

Funding. National Natural Science Foundation of China (NSFC) (11422434, 11621404); National Key Scientific Instrument Project (2012YQ150092); Shanghai Municipal Education Commission and Shanghai Education Development Foundation (16SG22).

REFERENCES

1. B. Schwarz, Nat. Photonics **4**, 429 (2010).
2. E. Baumann, F. R. Giorgetta, J. D. Deschênes, W. C. Swann, I. Coddington, and N. R. Newbury, Opt. Express **22**, 24914 (2014).
3. H. Zhou, Y. He, L. You, S. Chen, W. Zhang, J. Wu, Z. Wang, and X. Xie, Opt. Express **23**, 14603 (2015).
4. Y. Lin and L. Duan, IEEE Photon. Technol. Lett. **27**, 1761 (2015).
5. A. B. Mateo and Z. W. Barber, Appl. Opt. **54**, 5911 (2015).
6. S. Hyun, M. Choi, B. J. Chun, S. Kim, S. W. Kim, and Y. J. Kim, Opt. Express **21**, 9780 (2013).
7. W. Xia and X. Chen, Meas. Sci. Technol. **27**, 041001 (2016).
8. S. A. van den Berg, S. T. Persijn, G. J. P. Kok, M. G. Zeitouny, and N. Bhattacharya, Phys. Rev. Lett. **108**, 183901 (2012).
9. J. Lee, Y. J. Kim, K. Lee, S. Lee, and S. W. Kim, Nat. Photonics **4**, 716 (2010).
10. H. Wu, F. Zhang, F. Meng, T. Liu, J. Li, L. Pan, and X. Qu, Meas. Sci. Technol. **27**, 015202 (2016).
11. I. Coddington, W. C. Swann, L. Nenadovic, and N. R. Newbury, Nat. Photonics **3**, 351 (2009).
12. T. Kato, M. Uchida, and K. Minoshima, Sci. Rep. **7**, 3670 (2017).
13. K. Minoshima, H. Matsumoto, Z. Zhang, and T. Yagi, Jpn. J. Appl. Phys. **33**, L1348 (1994).
14. T. Ideguchi, S. Holzner, B. Bernhardt, G. Guelachvili, N. Picqué, and T. W. Hänsch, Nature **502**, 355 (2013).
15. J. Lee, S. Han, K. Lee, E. Bae, S. Kim, S. Lee, S. W. Kim, and Y. J. Kim, Meas. Sci. Technol. **24**, 045201 (2013).
16. H. Zhang, H. Wei, X. Wu, H. Yang, and Y. Li, Opt. Express **22**, 6597 (2014).
17. D. Yelin, I. Rizvi, W. M. White, J. T. Motz, T. Hasan, B. E. Bouma, and G. J. Tearney, Nature **443**, 765 (2006).
18. K. Goda, K. K. Tsia, and B. Jalali, Nature **458**, 1145 (2009).
19. A. Zeidan and D. Yelin, Biomed. Opt. Express **7**, 392 (2016).
20. C. Lei, B. Guo, Z. Cheng, and K. Goda, Appl. Phys. Rev. **3**, 011102 (2016).
21. A. Mahjoubfar, K. Goda, A. Ayazi, A. Fard, S. H. Kim, and B. Jalali, Appl. Phys. Lett. **98**, 101107 (2011).
22. A. Mahjoubfar, C. Chen, K. R. Niazi, S. Rabizadeh, and B. Jalali, Biomed. Opt. express **4**, 1618 (2013).
23. E. Hase, T. Minamikawa, S. Miyamoto, R. Ichikawa, Y. Hsieh, K. Shibuya, Y. Nakajima, A. Asahara, K. Minoshima, Y. Mizutani, T. Iwata, H. Yamamoto, and T. Yasui, "Scan-less confocal phase microscopy based on dual comb spectroscopy of two-dimensional-image-encoding optical frequency comb," preprint arXiv: 1705.07236 (2017).
24. E. Hase, T. Minamikawa, S. Miyamoto, H. Yamamoto, and T. Yasui, Proc. SPIE **76**, 100760X (2017).
25. D. Luo, W. Li, Y. Liu, C. Wang, Z. Zhu, W. Zhang, and H. Zeng, Appl. Phys. Express **9**, 082702 (2016).
26. K. K. Tsia, K. Goda, D. Capewell, and B. Jalali, Opt. Express **18**, 10016 (2010).

49.52.25.227 {ts '2018-08-12 22:50:48'}